

Non-linear Least Square Fitting Technique for the Determination of Field Line Resonance Frequency in Ground Magnetometer Data: Application to Remote Sensing of Plasmaspheric Mass Density

Athanasios Boudouridis¹, Endawoke Yizengaw², Mark Moldwin³, and Eftyhia Zesta⁴

¹Space Sciences Institute

²The Aerospace Corporation

³University of Michigan

⁴NASA Goddard Space Flight Center

November 21, 2022

Abstract

The accurate determination of the Field Line Resonance (FLR) frequency of a resonating geomagnetic field line is necessary to remotely monitor the plasmaspheric mass density during geomagnetic storms and quiet times alike. Under certain assumptions the plasmaspheric mass density at the equator is inversely proportional to the square of the FLR frequency. The most common techniques to determine the FLR frequency from ground magnetometer measurements are the amplitude ratio and phase difference techniques, both based on geomagnetic field observations at two latitudinally separated ground stations along the same magnetic meridian. Previously developed automated techniques have used statistical methods to pinpoint the FLR frequency using the amplitude ratio and phase difference calculations. We now introduce a physics-based automated technique, using non-linear least square fitting of the ground magnetometer data to the analytical resonant wave equations, that reproduces the wave characteristics on the ground, and from those determine the FLR frequency. One of the advantages of the new technique is the estimation of physics-based errors of the FLR frequency, and as a result of the equatorial plasmaspheric mass density. We present analytical results of the new technique, and test it using data from the Inner-Magnetospheric Array for Geospace Science (iMAGS) ground magnetometer chain along the coast of Chile and the east coast of the United States. We compare the results with the results of previously published statistical automated techniques.

Hosted file

essoar.10503693.1.docx available at <https://authorea.com/users/528557/articles/596895-non-linear-least-square-fitting-technique-for-the-determination-of-field-line-resonance-frequency-in-ground-magnetometer-data-application-to-remote-sensing-of-plasmaspheric-mass-density>

1 **Non-linear Least Square Fitting Technique for the Determination of**
2 **Field Line Resonance Frequency in Ground Magnetometer Data:**
3 **Application to Remote Sensing of Plasmaspheric Mass Density**
4

5 **A. Boudouridis^{1,2,3}, E. Yizengaw⁴, M. B. Moldwin⁵, and E. Zesta⁶**

6 ¹Space Sciences Institute, Boulder, CO, USA, ²Cooperative Institute for Research in
7 Environmental Sciences, University of Colorado, Boulder, CO, USA, ³National Center for
8 Environmental Information, National Oceanic and Atmospheric Administration, Boulder, CO,
9 USA, ⁴The Aerospace Corporation, El Segundo, CA, USA, ⁵University of Michigan, Ann Arbor,
10 MI, USA, ⁶NASA Goddard Space Flight Center, Greenbelt, MD, USA
11

12 Corresponding author: Athanasios Boudouridis (thanasis@spacescience.org)

13 **Key Points:**

- 14 • Physics-based Field Line Resonance (FLR) frequency determination technique
15 • Non-linear least squares fitting of analytical wave equations
16 • Physics-based FLR frequency and plasmaspheric mass density errors

17 Abstract

18 The accurate determination of the Field Line Resonance (FLR) frequency of a resonating
19 geomagnetic field line is necessary to remotely monitor the plasmaspheric mass density during
20 geomagnetic storms and quiet times alike. Under certain assumptions the plasmaspheric mass
21 density at the equator is inversely proportional to the square of the FLR frequency. The most
22 common techniques to determine the FLR frequency from ground magnetometer measurements
23 are the amplitude ratio and phase difference techniques, both based on geomagnetic field
24 observations at two latitudinally separated ground stations along the same magnetic meridian.
25 Previously developed automated techniques have used statistical methods to pinpoint the FLR
26 frequency using the amplitude ratio and phase difference calculations. We now introduce a
27 physics-based automated technique, using non-linear least square fitting of the ground
28 magnetometer data to the analytical resonant wave equations, that reproduces the wave
29 characteristics on the ground, and from those determine the FLR frequency. One of the
30 advantages of the new technique is the estimation of physics-based errors of the FLR frequency,
31 and as a result of the equatorial plasmaspheric mass density. We present analytical results of the
32 new technique, and test it using data from the Inner-Magnetospheric Array for Geospace Science
33 (iMAGS) ground magnetometer chain along the coast of Chile and the east coast of the United
34 States. We compare the results with the results of previously published statistical automated
35 techniques.

36 1 Introduction

37 The Earth's plasmasphere is an important plasma region of the terrestrial magnetosphere-
38 ionosphere system, playing a significant role in the dynamics of the magnetosphere-ionosphere
39 coupling during quiet and active periods alike (Lemaire & Gringauz, 1998; Goldstein et al.,
40 2004; Yizengaw & Moldwin, 2005; Kotova, 2007; Darrouzet et al., 2009; Masson et al., 2009;
41 Reinisch et al., 2009; Moldwin et al., 2016). During magnetic storms the mass loading and
42 unloading of the plasmasphere is an integral part of the storm process, with widespread
43 implications for a variety of processes in the magnetosphere and/or ionosphere (Sheeley et al.,
44 2001; Yizengaw et al., 2005). Earthward looking Extreme-UltraViolet (EUV) imagers on
45 spacecraft high above the magnetic pole have yielded valuable information of the structure of the
46 plasmasphere in recent decades (e.g., Goldstein, 2006; Goldstein et al., 2003, and references
47 therein).

48 The equatorial plasmaspheric mass density, ρ_{eq} , is a key parameter that tracks the
49 evolution of the plasmasphere during a magnetic storm or quiet periods. A simple, cost effective
50 technique that can measure ρ_{eq} at a specific L value (and provide large scale temporal coverage),
51 relies on the remote sensing of the plasmasphere using a pair of longitudinally aligned ground
52 magnetometers. This method is based on the relation between the wave period, T , of a resonating
53 magnetic field line and the mass density along this field line (Dungey, 1954), assuming
54 theoretically determined properties of wave amplitude and phase across the latitudinal spread of
55 the resonating bundle of fluxtubes. The standing waves on a closed magnetic field line are
56 referred to as a Field Line Resonance (FLR). FLR frequencies belong to the Ultra-Low
57 Frequency (ULF) range, typically in the Pc5 frequency range (1-10 mHz) within the auroral
58 zone, and in the Pc3/4 range (7-100 mHz or periods of 10-150 s) within the sub-auroral and
59 plasmasphere regions.

60 According to the Wentzel–Kramers–Brillouin (WKB) time of flight approximation in the
 61 solution of the standing wave equation (Gul’yel’mi, 1967; Kitamura & Jacobs, 1968; Schulz,
 62 1996; Menk et al., 1999; Denton & Gallagher, 2000, and references therein), the period of the
 63 standing wave along a magnetic fluxtube is given by

$$64 \quad T = \frac{2}{n} \int \frac{ds}{V_A} = \frac{2}{n} \int \frac{ds}{B/(\mu_o \rho)^{1/2}} \quad (1)$$

65 where n is the wave mode number, V_A the Alfvén speed, s the distance along the magnetic field
 66 line, B the magnetic field, ρ the mass density all along the field line, and μ_o the permeability of
 67 free space. The mass density ρ along the field lines is usually represented as a power law
 68 decrease with radial distance R

$$69 \quad \rho = \rho_{eq} \left(\frac{LR_E}{R} \right)^m \quad (2)$$

70 where R is the radial distance from the center of the Earth, L is the equatorial radial distance of a
 71 fluxtube in Earth radii R_E , and m is the power law index of the density decrease along the field
 72 lines. Following Schultz (1996), and assuming a dipole magnetic field, equations (1) and (2)
 73 yield the value of the equatorial plasmaspheric mass density as

$$74 \quad \rho_{eq} = 4.4794 \times 10^7 \frac{\left(\frac{3}{\sin(I_L)} + \frac{1}{I_M} \right)^2}{L^8 f_{FLR}^2} \quad (3)$$

$$75 \quad I_L = \cos^{-1} \left(\sqrt{\frac{1}{L}} \right) \quad (4)$$

$$76 \quad I_M = \frac{(3I_L + L^{-3/2})(3L + 2)\sin(I_L)}{8} \quad (5)$$

77 where f_{FLR} is the FLR frequency. The above equations show that knowledge of the FLR
 78 frequency can yield ρ_{eq} at the L value of the observing ground station.

79 Observations have shown that FLRs are present in the inner magnetosphere down to L
 80 values of 1.5 (Menk et al., 1994, 2000). For L values lower than that, most of the magnetic field
 81 line lies within the dense ionosphere, and thus the ULF oscillations on that field line are strongly
 82 damped. Many techniques have been developed to obtain the FLR frequency of the resonating
 83 field lines (Baransky et al., 1985, 1990; Waters et al., 1991, 1994; Pilipenko & Fedorov, 1994;
 84 Menk et al., 1999, 2000). In the current study we will use the amplitude ratio (AR), and cross-
 85 phase or phase difference (CP or PD) techniques. Both techniques rely on measurements from
 86 two adjacent ground stations, at approximately the same magnetic longitude, and separated by
 87 less than 200 km in magnetic latitude.

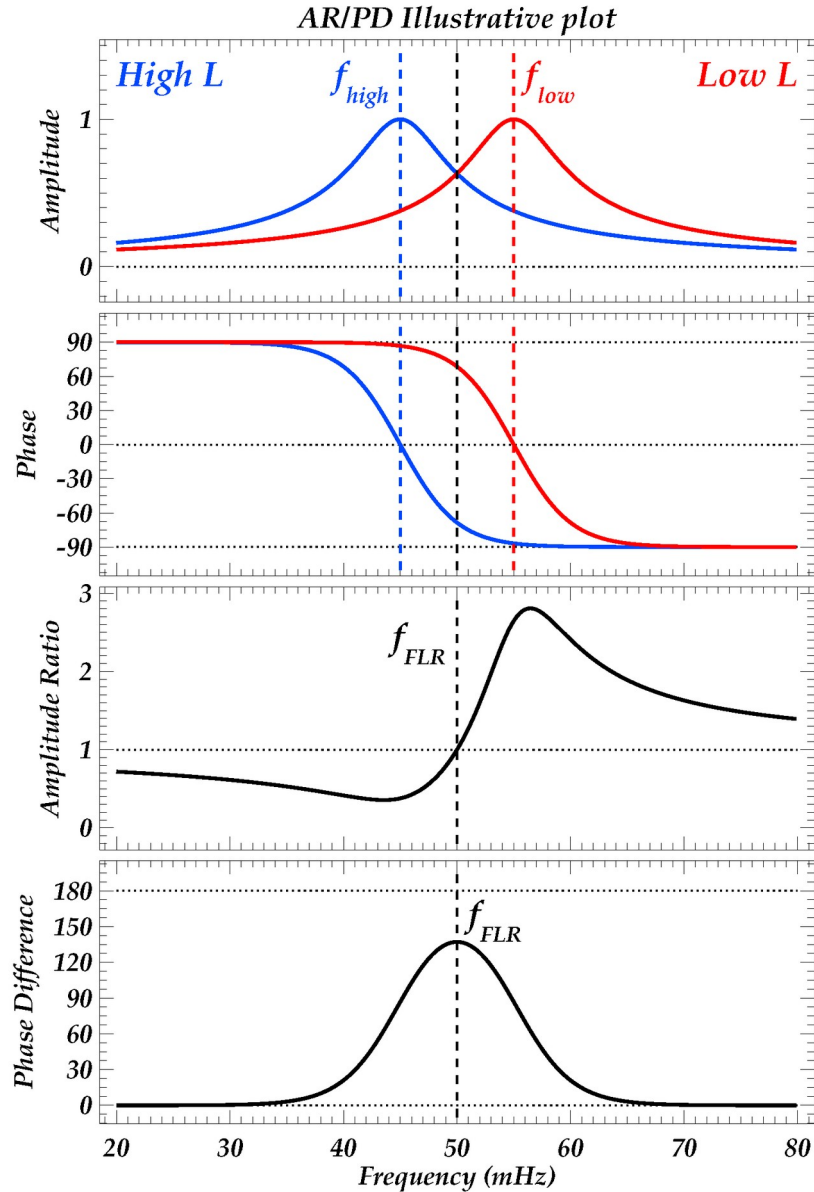


Figure 1. Illustrative plot of the AR and PD methodologies in determining the FLR frequency of the waves at the mid-point of a longitudinally aligned station pair. From top to bottom the four panels show the wave amplitude at the two stations, the wave phase, the amplitude ratio, and the phase difference.

88 The techniques are described in detail in Boudouridis & Zesta (2007), and illustrated in
 89 Figure 1. Briefly, assuming a latitudinally uniform distribution of resonating field lines according
 90 to (1), the FLR frequency of the waves decreases as the field line length increases, therefore the
 91 FLR frequency is decreasing with increasing latitude (Menk et al., 1994). At every latitude, the
 92 wave amplitude exhibits a maximum at the FLR frequency of that field line (Figure 1, panel 1
 93 from top), while the wave phase reverses, shifts by 180° (panel 2 from top) across the latitude of
 94 the resonance. For two adjacent in latitude magnetometer stations, the ratio of their wave
 95 amplitudes (AR) has a transition through 1 (panel 3 from top), while the difference of their wave
 96 phases (PD) demonstrates a maximum value (panel 4 from top), at the frequency half way
 97 between the peak amplitude frequencies of the two stations. Since for two stations in close

98 proximity to each other the frequency decreases almost linearly with increasing latitude, the mid-
99 point frequency is the FLR frequency at the mid-point latitude between the stations. The two
100 frequency values, one from AR and one from PD, yield two independent measurements of the
101 FLR frequency for the L value of the mid-point between the two stations. A chain of
102 longitudinally aligned magnetometers can thus observe the FLR frequency at a range of L values,
103 as many as the number of pairs of stations that can be formed between the existing stations of the
104 chain. As the Earth rotates the chain measures the latitudinal distribution of the FLR frequency at
105 all magnetic local times (MLTs), as long as there are waves present in the magnetosphere. This
106 ultimately yields the radial distribution of the equatorial plasmaspheric mass density (Chi et al.,
107 2013).

108 2 Analytical FLR Determinations

109 The two FLR detection techniques mentioned above have been automated, using
 110 statistical methods to pinpoint the FLR frequency (Berube et al., 2003; Boudouridis & Zesta,
 111 2007). The first steps involve generation of the dynamic spectra of the magnetic observations
 112 from the two stations, and calculation of the AR and PD for the station pair, for the frequency
 113 range around resonances, typically the Pc3/4 ULF range for the plasmasphere. Subsequent steps
 114 (detailed in Boudouridis & Zesta (2007)) include smoothing of the AR and PD in two
 115 dimensions (frequency vs time), and application of various statistical manipulations of the data,
 116 such as the t-test to estimate a meaningful maximum of the PD, or time-constant ratio of the
 117 average amplitude at two frequency ranges to estimate the transition through 1 of the AR, at the
 118 desired time step through the data. The end result is two curves, one for AR and one for PD, of
 119 derived FLR frequencies as a function of time during the period of ULF wave presence, typically
 120 in the dayside magnetosphere (Boudouridis & Zesta, 2007, their figures 2 and 3).

121 The statistical methods used for the FLR frequency determination yield reasonably good
 122 results whenever there is sufficient Pc3/4 ULF wave power present. This occurs mostly on the
 123 dayside magnetosphere. Despite their success in pinpointing the FLR frequency in magnetometer
 124 data from a pair of ground stations, the statistical techniques use ad hoc detection criteria that
 125 lack the robustness of a physics-based technique. The analytical, physics-based technique that we
 126 present in this paper uses the analytical standing wave equations to calculate the expected AR
 127 and PD for the station pair, and then fit them to the data at the desired time resolution. At each
 128 time step the transition through 1 of the AR, and the maximum of the PD can be calculated from
 129 the resulting analytical curves, yielding the time evolution of the FLR frequency for the two FLR
 130 determination techniques. The additional advantage of the new analytical technique is the
 131 estimation of physics-based errors of the FLR frequency and the equatorial plasmaspheric mass
 132 density.

133 2.1 ULF wave equations and AR/PD fitting

134 Following Kawano et al. (2002), the wave phase, Φ_{low} , and amplitude, H_{low} , of a standing
 135 wave at the lower latitude station of the station pair, as a function of frequency, are given by

$$136 \quad \Phi_{low} = \tan^{-1} \left(\frac{f - a_1}{a_0} \right) \quad (6)$$

$$137 \quad H_{low} = \frac{b_0}{\sqrt{1 + \frac{(f - b_2)^2}{b_1}}} \quad (7)$$

138 where f is the wave frequency, and the parameters $[a_i, b_j]$ define the wave characteristics as
 139 follows (refer to Figure 1): a_1 represents the phase reversal frequency, a_0 is a measure of the
 140 phase reversal rate with frequency, b_2 represents the frequency of the peak amplitude, b_1 is a
 141 measure of the amplitude change rate with frequency, and b_0 is the peak wave amplitude.
 142 Similarly, the wave equations for the higher latitude station are given by

$$143 \quad \Phi_{high} = \tan^{-1} \left(\frac{f - a_3}{a_2} \right) \quad (8)$$

144
$$H_{high} = \frac{b_3}{\sqrt{1 + \frac{(f - b_5)^2}{b_4}}} \quad (9)$$

145 The phase difference $\Delta\Phi$, and amplitude ratio H_r , for the station pair are given, respectively, by
146 equations

147
$$\Delta\Phi = \Phi_{low} - \Phi_{high} \quad (10)$$

148
$$H_r = \frac{H_{low}}{H_{high}} \quad (11)$$

149 This convention yields a maximum PD at the midpoint between stations, and a transition from
150 lower to higher than 1 value for the AR at the same location, since the frequency of the standing
151 waves decreases with increasing latitude as mentioned earlier (Menk et al., 1994). With this
152 parameterization, equation (10) has 4 free parameters, $a_i(i=0,\dots,3)$, and equation (11) has 6
153 free parameters, $b_i(i=0,\dots,5)$. These free parameters can be determined by non-linear least
154 square fitting of the PD and AR data as a function of frequency at every step in time, using the
155 analytical equations (6)-(11).

156 Figure 2 demonstrates the application of the analytical technique to a station pair located
157 at Puerto Natales (PNT) and Punta Arenas (PAC) in Southern Chile. Comparison with the
158 statistical results of Boudouridis & Zesta (2007) are also shown in Figure 2. Panels 1 and 3 from
159 the top show the PD and AR of the pair for the time period 1300-1600 UT on 21 December 2003,
160 as a function of time and frequency, color coded with the scales on the right of each panel. These
161 are calculated from the ground magnetic field data observed at PNT and PAC. The horizontal
162 black lines in panels 1 and 3 denote the maximum PD and AR transition through 1, respectively,
163 determined with the statistical methods of Boudouridis & Zesta (2007) at 1-min intervals.

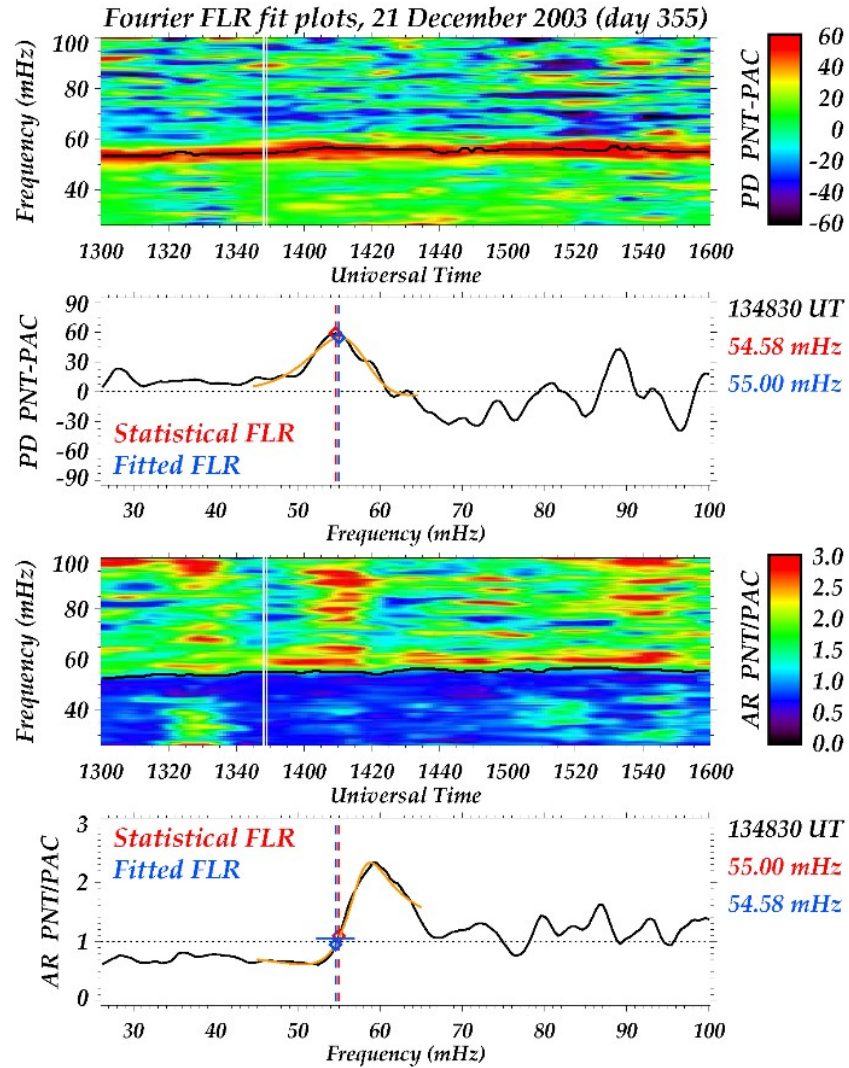


Figure 2. Analytical fit of wave PD and AR from two adjacent stations, FLR frequency determination (with estimated errors), and comparison with statistical determinations.

164 Panels 2 and 4 from the top show the results of the non-linear least square fitting of
 165 equations (10) and (11) to the observed PD and AR, respectively, for one such 1-min interval,
 166 1348-1349 UT, denoted by the vertical white lines in panels 1 and 3. The black lines in panels 2
 167 and 4 are the corresponding measured PD and AR (from the color-coded displays of panels 1 and
 168 3) plotted as a function of frequency for this 1-min interval. The orange lines are the
 169 corresponding non-linear least square fits of the black curves with the functions of equations (10)
 170 and (11). The red diamonds in the two panels mark the statistical PD maximum/AR transition
 171 through 1 using the methodology of Boudouridis & Zesta (2007). The blue diamonds denote the
 172 fitted PD maximum/AR transition through 1, using the new analytical technique. The vertical
 173 dashed lines and captions on the right of the panels, of the same colors, show the FLR
 174 frequencies determined with the two methods. The same procedure is applied for every minute of
 175 the interval shown, 1300-1600 UT. This yields the analytical equivalent of the statistical FLR
 176 frequency determinations (black horizontal lines) of panels 1 and 3. Figure 3, top panel, shows
 177 the statistically and analytically determined FLRs for both the PD and AR techniques at 1-min

178 intervals across the same time period as in Figure 2. We discuss these results in more detail
179 below.

180 2.2 FLR errors

181 A further advantage of the new technique is the estimation of physics-based errors of the
182 FLR frequency, which can yield physics-based errors of the equatorial plasmaspheric mass
183 density. These are the result of error propagation from the fitting parameter errors. Considering
184 that the two stations are in close proximity, the change of FLR frequency with latitude between
185 them is approximately linear. Therefore, the resulting midpoint PD and AR FLR frequencies,
186 respectively, are given by the average of the corresponding fitted parameters that represent the
187 FLR frequencies in equations (6)-(9)

$$188 \quad f_{PD} = \frac{a_1 + a_3}{2} \quad (12)$$

$$189 \quad f_{AR} = \frac{b_2 + b_5}{2} \quad (13)$$

190 The fitting parameter errors, Δa_i and Δb_i , are determined by the nonlinear least square fitting
191 technique. As a result, the respective errors, Δf_{PD} and Δf_{AR} , can be defined as

$$192 \quad \Delta f_{PD} = \frac{\Delta a_1 + \Delta a_3}{2} \quad (14)$$

$$193 \quad \Delta f_{AR} = \frac{\Delta b_2 + \Delta b_5}{2} \quad (15)$$

194 The resulting errors are shown as blue horizontal bars on the fitted FLR frequencies (blue
195 diamonds), on panels 2 and 4 from the top of Figure 2. (Note that the error of the PD technique
196 (panel 2) is present but not visible as it is very small).

197 3 Plasmaspheric Mass Density

198 Once the FLR frequency is known, the plasmaspheric mass density can be calculated
199 through equations (3)-(5). Equation (3) also yields the error in ρ_{eq} as

$$200 \quad \Delta \rho_{eq} = \frac{-2 \rho_{eq} \Delta f}{f} \quad (16)$$

201 where Δf is either Δf_{PD} or Δf_{AR} from equations (14) and (15), respectively. The results for the
202 interval 1300-1600 UT on 21 December 2003, and station pair PNT/PAC are shown in Figure 3.
203 The top panel shows the FLR frequencies, old statistical CP (red), old statistical AR (blue), new
204 fitted CP (black), and new fitted AR (orange). The bottom panel shows the corresponding mass
205 density determinations in amu/cc. The errors of the new technique are shown as vertical orange
206 bars for the AR method, and black bars for the CP method (barely visible in most instances). The
207 CP error is <1% while the AR error is in the range of 10-15%. Clearly the CP method has much
208 smaller errors. The corresponding mass density errors are 0.1-1% for the CP method, and 5-18%
209 for the AR method.

210 4

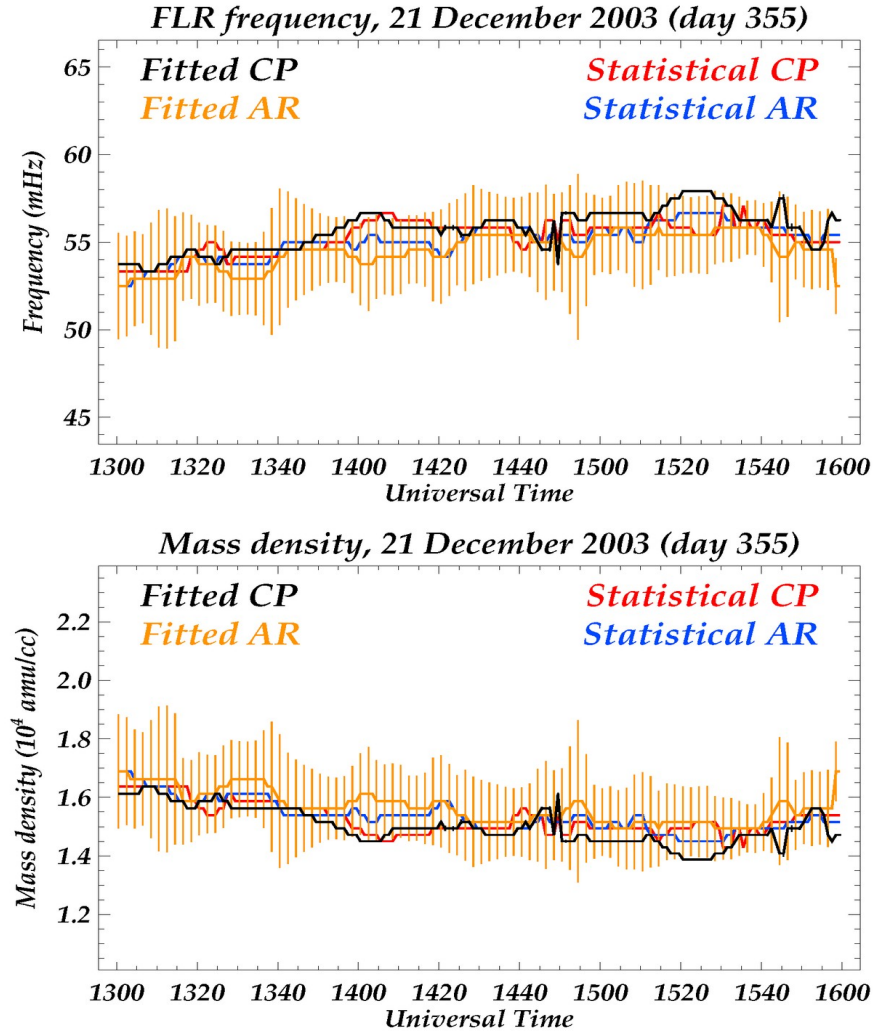


Figure 3. Application of the fit for 1300-1600 UT on 21 December 2003.

211 Conclusions

212 In this work we described two physics-based, AR and PD, FLR frequency determination
 213 techniques. At the heart of the new methods is the non-linear least square fitting of the AR and
 214 PD data, as opposed to statistical manipulations of this data. The analytical approach introduces
 215 physics-based errors of the FLR frequency, and of the equatorial plasmaspheric mass density.
 216 The results show that these errors are much smaller for the PD technique compared to the AR
 217 technique, both for the FLR frequency and the equatorial plasmaspheric mass density.

218 The present approach can be further improved. Some future directions are the following:

- 219 1. Introduction of criteria for the convergence or not of the non-linear least square fitting for the
 220 two techniques, AR and PD, in order to eliminate erroneous results.
- 221 2. Use of criteria for the comparison of the AR and PD methods, in order to exclude frequencies
 222 for which the two techniques yield very different results.

- 223 3. The results of the analytical non-linear least square fitting technique depend on the initial
 224 choice of the fit parameters a_i and b_i . This is especially true for the AR technique, but to a
 225 lesser extent for the PD technique as well. Currently these parameters are chosen manually at
 226 the beginning of the automated procedure, and are applied at every minute of the entire test
 227 interval. Instead, these parameters can be selected interactively, different at every minute of
 228 the test interval, in an effort to minimize the errors of the fit, and thus the errors of the FLR
 229 frequency and equatorial plasmaspheric mass density.
- 230 4. Use of a more realistic magnetic field model, such as the Tsyganenko T01 model (Berube et
 231 al., 2006).

232 **Acknowledgments, Samples, and Data**

233 The work by Athanasios Boudouridis at the Space Science Institute (SSI) was supported
 234 by NSF awards AGS-1450512 and AGS-1848730. Mark Moldwin was supported by NSF
 235 awards AGS-1450512 and AGS-1654044. The ground magnetometer data are available at [http://](http://magnetometers.bc.edu)
 236 magnetometers.bc.edu.

237 **References**

- 238 Baransky, L. N., Borovkov, Y. E., Gokhberg, M. B., Krylov, S. M., & Troitskaya V. A. (1985).
 239 High resolution method of direct measurement of the magnetic field lines'
 240 eigenfrequencies. *Planet. Space Sci.*, *33*, 1369–1374.
- 241 Baransky, L. N., Belokris, S. P., Borovkov, Y. E., & Green C. A. (1990). Two simple methods for
 242 the determination of the resonance frequencies of magnetic field lines. *Planet. Space Sci.*,
 243 *38*, 1573–1576.
- 244 Boudouridis, A., & Zesta, E. (2007). Comparison of Fourier and wavelet techniques in the
 245 determination of geomagnetic field line resonances. *J. Geophys. Res.*, *112*, A08205,
 246 <https://doi.org/10.1029/2006JA011922>
- 247 Berube, D., Moldwin, M. B., & Weygand, J. M. (2003). An automated method for the detection
 248 of field line resonance frequencies using ground magnetometer techniques. *J. Geophys.*
 249 *Res.*, *108*(A9), 1348, <https://doi.org/10.1029/2002JA009737>
- 250 Berube, D., Moldwin, M. B., & Ahn, M. (2006). Computing magnetospheric mass density from
 251 field line resonances in a realistic magnetic field geometry. *J. Geophys. Res.*, *111*,
 252 A08206, <https://doi.org/10.1029/2005JA011450>
- 253 Chi, P. J., et al. (2013). Sounding of the plasmasphere by Mid-continent MAgnetoseismic Chain
 254 (McMAC) magnetometers. *J. Geophys. Res. Space Physics*, *118*, 3077–3086,
 255 <https://doi.org/10.1002/jgra.50274>
- 256 Darrouzet, F., Gallagher, D. L., André, N., Carpenter, D. L., Dandouras, I., Décréau, P. M. E., De
 257 Keyser, J., Denton, R. E., Foster, J. C., Goldstein, J., Moldwin, M. B., Reinisch, B.W.,
 258 Sandel, B. R., & Tu, J. (2009). Plasmaspheric density structures and dynamics: Properties
 259 observed by the CLUSTER and IMAGE missions. *Space Sci. Rev.*, *145*, 55–106,
 260 <https://doi.org/10.1007/s11214-008-9438-9>
- 261 Denton, R. E., & Gallagher, D. L. (2000). Determining the mass density along magnetic field
 262 lines from toroidal eigenfrequencies. *J. Geophys. Res.*, *105*, 27,717–27,725.

- 263 Dungey, J. W. (1954). The attenuation of Alfvén waves. *J. Geophys. Res.*, *59*(3), 323–328,
264 <https://doi.org/10.1029/JZ059i003p00323>
- 265 Goldstein, J. (2006). Plasmasphere response: Tutorial and review of recent imaging results.
266 *Space Sci. Rev.*, *124*, 203–216, <https://doi.org/10.1007/s11214-006-9105-y>
- 267 Goldstein, J., Spasojević, M., Reiff, P. H., Sandel, B. R., Forrester, W. T., Gallagher, D. L., &
268 Reinisch, B. W. (2003). Identifying the plasmopause in IMAGE EUV data using IMAGE
269 RPI in situ steep density gradients. *J. Geophys. Res.*, *108*(A4), 1147,
270 <https://doi.org/10.1029/2002JA009475>
- 271 Goldstein, J., Sandel, B. R., Hairston, M. R., & Mende, S. B. (2004). Plasmopause undulation of
272 17 April 2002. *Geophys. Res. Lett.*, *31*, L15801, <https://doi.org/10.1029/2004GL019959>
- 273 Gul'yel'mi, A. V. (1967). Theory of hydromagnetic sounding of plasma concentration in the
274 exosphere. *Geomagn. Aeron.*, *7*, 357–363.
- 275 Kawano, H., Yumoto, K., Pilipenko, V. A., Tanaka, Y.-M., Takasaki, S., Iizima, M., & Seto M.
276 (2002). Using two ground stations to identify magnetospheric field line eigenfrequency as
277 a continuous function of ground latitude. *J. Geophys. Res.*, *107*(A8), 1202,
278 <https://doi.org/10.1029/2001JA000274>
- 279 Kitamura, T., & Jacobs, J. A. (1968). Determination of the magnetospheric plasma density by the
280 use of long-period geomagnetic micropulsations. *J. Geomagn. Geoelectr.*, *20*, 33–44.
- 281 Kotova, G. A. (2007). The Earth's Plasmasphere: State of Studies (a Review). *Geomagn. Aeron.*,
282 *47*, 409–422.
- 283 Lemaire, J. F., & Gringauz, K. I. (1998). *The Earth's Plasmasphere*. Cambridge University Press,
284 New York.
- 285 Masson, A., Santolík, O., Carpenter, D. L., Darrouzet, F., Décréau, P. M. E., El-Lemdani
286 Mazouz, F., Green, J. L., Grimald, S., Moldwin, M. B., Němec, F., & Sonwalkar, V. S.
287 (2009). Advances in plasmaspheric wave research with CLUSTER and IMAGE
288 observations. *Space Sci. Rev.*, *145*, 137–191, <https://doi.org/10.1007/s11214-009-9508-7>
- 289 Menk, F. W., Fraser, B. J., Waters, C. L., Ziesolleck, C. W. S., Feng, Q., Lee, S. H., & McNabb,
290 P. W. (1994). Ground measurements of low latitude magnetospheric field line resonances.
291 In *Solar Wind Sources of Magnetospheric Ultra-Low Frequency Waves*, *Geophys.*
292 *Monogr. Ser.*, vol. 81, edited by M. J. Engebretson, K. Takahashi, and M. Scholer, pp.
293 299–310, AGU, Washington D. C.
- 294 Menk, F. W., Orr, D., Clilverd, M. A., Smith, A. J., Waters, C. L., Milling, D. K., & Fraser, B. J.
295 (1999). Monitoring spatial and temporal variations in the dayside plasmasphere using
296 geomagnetic field line resonances. *J. Geophys. Res.*, *104*, 19,955–19,969.
- 297 Menk, F. W., Waters, C. L., & Fraser, B. J. (2000). Field line resonances and waveguide modes at
298 low latitudes: 1. Observations. *J. Geophys. Res.*, *105*, 7747–7761.
- 299 Moldwin, M. B., Zou, S., & Heine, T. (2016). The story of plumes: the development of a new
300 conceptual framework for understanding magnetosphere and ionosphere coupling. *Ann.*
301 *Geophys.*, *34*, 1243–1253, <https://doi.org/10.5194/angeo-34-1243-2016>

- 302 Pilipenko, V. A., & Fedorov, E. N. (1994). Magnetotelluric sounding of the crust and
303 hydrodynamic monitoring of the magnetosphere with the use of ULF waves. In *Solar*
304 *Wind Sources of Magnetospheric Ultra-Low Frequency Waves*, *Geophys. Monogr. Ser.*,
305 vol. 81, edited by M. J. Engebretson, K. Takahashi, and M. Scholer, pp. 283–292, AGU,
306 Washington D. C.
- 307 Reinisch, B. W., Moldwin, M. B., Denton, R. E., Gallagher, D. L., Matsui, H., Pierrard, V., & Tu,
308 J. (2009). Augmented empirical models of plasmaspheric density and electric field using
309 IMAGE and CLUSTER Data. *Space Sci. Rev.*, *145*, 231–261,
310 <https://doi.org/10.1007/s11214-008-9481-6>
- 311 Schulz, M. (1996). Eigenfrequencies of geomagnetic field lines and implications for plasma-
312 density modeling. *J. Geophys. Res.*, *101*, 17,385–17,397.
- 313 Sheeley, B. W., Moldwin, M. B., Rassoul, H. K., & Anderson, R. R. (2001). An empirical
314 plasmasphere and trough density model: CRRES observations. *J. Geophys. Res.*, *106*,
315 25,631–25,641.
- 316 Waters, C. L., Menk, F. W., & Fraser, B. J. (1991). The resonance structure of low latitude Pc3
317 geomagnetic pulsations. *Geophys. Res. Lett.*, *18*, 2293–2296.
- 318 Waters, C. L., Menk, F. W., & Fraser, B. J. (1994). Low latitude geomagnetic field line
319 resonance: Experiment and modeling. *J. Geophys. Res.*, *99*, 17,547–17,558.
- 320 Yizengaw, E., & Moldwin, M. B. (2005). The altitude extension of the mid-latitude trough and
321 its correlation with plasmopause position. *Geophys. Res. Lett.*, *32*, L09105,
322 <https://doi.org/10.1029/2005GL022854>
- 323 Yizengaw, E., Wei, H., Moldwin, M. B., Galvan, D., Mandrake, L. L., Mannucci, A., & Pi, X.
324 (2005). The correlation between mid-latitude trough and the plasmopause. *Geophys. Res.*
325 *Lett.*, *32*, L10102, <https://doi.org/10.1029/2005GL022954>